A missense mutation in zinc finger homeobox-3 (ZFHX3) impedes growth and alters metabolism and hypothalamic gene expression in mice.

Patrick M. Nolan [1] *, Gareth Banks [1], Nora Bourbia [1, 2], Ashleigh G. Wilcox [1], Liz Bentley [3], Lee Moir [3], Lee Kent [3], Rosie Hillier [3], Dana Wilson [4], Perry Barrett [4], Rebecca Dumbell [1, 5] *

1. Mammalian Genetics Unit, MRC Harwell Institute, Oxfordshire, UK

2. Current Address: UK Health Security Agency, Radiation, Chemical and Environmental Hazards Directorate, Chilton, Oxfordshire, UK

3. Mary Lyon Centre at MRC Harwell, Oxfordshire, UK

4. The Rowett Institute, University of Aberdeen, Aberdeen, UK

5. School of Science and Technology, Department of Biosciences, Nottingham Trent University, Nottingham, UK

* Corresponding authors

Highlights

- Male and female *Zfhx3*$^{Sci/+}$ mice have a shorter body length, eat less and weigh less
- *Zfhx3*$^{Sci/+}$ mice have lower insulin, leptin and IGF1 in circulation
- *Zfhx3*$^{Sci/+}$ mice have decreased *Ghr, Ghrh* and *Npy* expression in the arcuate nucleus
- Arcuate nucleus expression of AT-motif containing *Sst* is increased in *Zfhx3*$^{Sci/+}$ mice
- This model may explain human protein altering *ZFHX3* variant associated with low BMI

Abstract

Objective: A protein altering variant in the gene encoding zinc finger homeobox-3 (*ZFHX3*) has recently been associated with lower BMI in a human genome-wide association study. We investigated metabolic parameters in mice harbouring a missense mutation in *Zfhx3* (*Zfhx3*$^{Sci/+}$) and looked for altered expression of transcripts that are associated with energy balance in the hypothalamus to understand how ZFHX3 may influence metabolic effects.

Methods: Body weight, length and composition were measured in 1 year old male and female *Zfhx3*$^{Sci/+}$ and *Zfhx3*$^{+/+}$ mice, and fat depot weights were measured along with fasted anabolic hormone concentrations. In a second cohort of male and female *Zfhx3*$^{Sci/+}$ and *Zfhx3*$^{+/+}$ mice weekly food intake was measured from the age of 9 – 20 weeks. A third cohort of female-only *Zfhx3*$^{Sci/+}$ and *Zfhx3*$^{+/+}$ mice underwent body composition analysis every two weeks from 6 - 14 weeks of age, and 24 h energy expenditure was assessed. At 16 weeks old, brains were collected in the light and dark phases for mRNA *in situ* hybridisation analysis of candidate genes identified in previous RNA-seq analysis of hypothalamic tissue of *Zfhx3*$^{Sci/+}$ mice.

Results: We found that 1 year old *Zfhx3*$^{Sci/+}$ mice weighed less and had a shorter body length than wildtype littermates, and had reduced fat mass, smaller mesenteric fat depots, and lower circulating insulin, leptin and insulin-like growth factor-1 (IGF1) concentrations. Male and female *Zfhx3*$^{Sci/+}$ mice ate less than wildtype controls from 10 weeks of age. In the final experiment, female *Zfhx3*$^{Sci/+}$ mice weighed less and had lower lean mass, but fat mass didn't differ. Energy expenditure was lower in *Zfhx3*$^{Sci/+}$ mice. We detected increased expression of somatostatin, and decreased expression of growth hormone-releasing hormone and growth hormone-receptor mRNAs in the arcuate nucleus (ARC), but these transcripts were unaltered in other hypothalamic nuclei. Similarly, ARC expression of orexigenic neuropeptide Y was decreased and ventricular ependymal layer expression of orphan G protein-coupled receptor *Gpr50* was decreased.

Conclusions: The *Sci* missense mutation conferred a protective metabolic phenotype in mice and implied a somatic growth effect. The promoters of mouse *Sst* and *Gpr50* genes contain ZFHX3 binding AT-motifs, suggesting growth axis effects are driven by transcriptional activation of *Sst* in the ARC. It is likely that altered *Gpr50* gene expression led to decreased energy expenditure and decreased *Npy* expression in the ARC decreased appetite. Together these results point to a pleiotropic effect of ZFHX3 in regulating energy balance, independent of its circadian effects.

Keywords

zfhx3, atbf1, energy balance, appetite, growth, mouse model, somatostatin, Gpr50, IGF1

1. Introduction

Obesity is a major contributor to preventable death worldwide [1], with comorbidities including type 2 diabetes, cardiovascular disease and some cancers, while early data even suggest a link to higher morbidity in COVID-19 patients [2]. A genetic underpinning of body weight in humans has been demonstrated in twin and family studies [3], and genome wide association studies (GWAS) have identified over 250 common variants associated with obesity indicated by body mass index (BMI) in humans [4,5], however very few of the mechanisms behind these associations have been described. Despite this, pathway analyses indicate that the majority of BMI – associated variants are in genes expressed in the hypothalamus [4], the brain region classically associated with homeostatic regulation of appetite and energy expenditure [6], indicating the importance of hypothalamic homeostatic body weight regulation in the human population. A recent GWAS identified a low frequency (4.34 %) protein altering variant in *ZFHX3* (zinc-finger homeobox-3) associated with lower BMI (- 0.11 kg / m^2), linking this gene to human obesity for the first time. In the same study knockdown of the *Drosophila melanogaster* homologue (*zfh2*) in adipose and neuronal tissue led to increased triglyceride levels in these flies [7], implicating a conserved role for ZFHX3 and its homologues in body weight regulation.

ZFHX3, also called AT motif-binding factor-1 (ATBF1), was first described as a transcriptional regulator binding to an AT (adenine and thymine)-rich motif of the *AFP* gene [8], and suppressing transcription by inhibiting binding of activator proteins [9]. The mouse missense mutation "short circuit" (*Sci*) was identified in an *N*-ethyl-*N*-nitrosourea mutagenesis screen for circadian phenotypes and encodes a V1963F missense substitution in a highly conserved region in exon 9 of *Zfhx3* [10]. *Zfhx3* is expressed in discrete regions of the adult mouse brain including nuclei of the anterior hypothalamus such as the suprachiasmatic nucleus (SCN) and arcuate nucleus (ARC) [11]. Characterisation of the mouse missense mutant has implicated *Zfhx3* in SCN regulation of circadian rhythms. $Zfhx3^{Sci/+}$ mice housed in constant darkness exhibit a shortened circadian behavioural rhythm mediated by altered ZFHX3 binding to AT motifs in the promoters of *Avp* and *Vip* in the SCN while numerous other neuropeptide neurotransmitter and receptor levels were also misregulated [10]. This role for *Zfhx3* has been further demonstrated in an adult mouse induced knockout of *Zfhx3* [12], independent of any effects that may have been established throughout development, supporting the sustained role of this transcription factor in regulating neuroendocrine homeostasis.

RNA-seq analysis of hypothalamic tissue from $Zfhx3^{Sci/+}$ mice have revealed altered expression of several genes implicated in appetite, growth and energy expenditure. Many of these identified transcripts, including those encoding somatostatin (*Sst*) and G-protein coupled receptor-50 (*Gpr50*), contain the AT motif in their promoter, and ZFHX3-driven activity at such promoters is affected in the *Sci* mutation [10]. This is a potential, although heretofore unexplored, mechanism by which ZFHX3 may mediate whole body energy balance. Based on these previous findings, our study set out to investigate the role of ZFHX3 in hypothalamic transcriptional regulation of appetite, growth and energy expenditure pathways using aged and young adult $Zfhx3^{Sci/+}$ mice. By comparing these pathways in control and mutant mice, we identify a potential mechanism for ZFHX3 regulation of growth, appetite, and adiposity through growth axis component mRNA expression in the ARC. This demonstrates mechanisms by which ZFHX3 may regulate appetite and body weight, identifying pathways that may be targeted for therapeutic intervention.

2. Methods

2.1 Animals

All animal experiments were conducted according to Medical Research Council (MRC) guidance in Responsibility in the Use of Animals for Medical Research (July 1993), and UK Home Office Project Licences 30/3206 and P6165EED1, with local ethical approval. All mice were housed at the Mary Lyon Centre, MRC Harwell Institute and, unless otherwise stated, were mixed-genotype group housed in individually ventilated cages in a pathogen free environment, in a 12h:12h light:dark light cycle (LD 12:12; lights on at 0700) with *ad libitum* access to standard rodent chow (SDS Rat and Mouse No. 3 Breeding diet, RM3), and water. *Zfhx3*$^{Sci/+}$ mice, harbouring a V1963F missense mutation in the conserved region upstream of the 17th zinc-finger motif of ZFHX3, were maintained on a mixed C3H/HeH × C57BL6/J F1 background and genotyping was carried out by RT-PCR Taqman assay with the following primers and probes (5′ to 3′): FW TCCACGCATTGCTTCAGATG. REV TGTGCCTTCTGCTTGTTCTCA. Mutant probe VIC—TTTGAGCTCTTCATTCA. Wildtype probe FAM—CTTTGAGCTCGTCATT. Mice homozygous for this mutation show perinatal lethality and so only mice heterozygous for this mutation and their wildtype littermates were included in this study.

2.1.1 Experiment 1 – Year old mice

Male and female 12-month-old *Zfhx3*$^{Sci/+}$ and *Zfhx3*$^{+/+}$ mice (n = 9 – 12) underwent body composition analysis by quantitative NMR (Echo MRI, Echo Medical Systems), and the following week were fasted overnight, and humanely killed at 2 hours following lights on (zeitgeber time (ZT) 2) by overdose of anaesthesia. Under terminal anaesthesia, a retro-orbital bleed was carried out and serum collected, body length from nose to base of tail was measured and, on confirmation of death, left side fat tissues were dissected and weighed.

2.1.2 Experiment 2 – Food intake measurements and early weight gain

Male and female *Zfhx3*$^{Sci/+}$ and *Zfhx3*$^{+/+}$ mice were weaned into pair-housed sex and genotype matched cages from 8 weeks of age. Mice and food remaining in the hopper were weighed weekly up to 20 weeks of age. For the food intake measurements, the experimental unit was the cage (n = 5 – 6 per sex and genotype), with n = 10 – 12 mice in total per group. Body weight was not collected for all mice at 19 – 20 weeks of age, so these data are excluded from the analysis.

2.1.3 Experiment 3 – Growth and hypothalamic gene expression in young female mice

Since early differences were stronger in female mice, only this sex was used in the final experiment. Female *Zfhx3*$^{Sci/+}$ and *Zfhx3*$^{+/+}$ mice were weighed and underwent body composition analysis by quantitative NMR (Echo MRI, Echo Medical Systems, Houston, TX) every two weeks from 6 – 14 weeks of age (n = 24 – 26). 5 mice did not undergo measurement at week 14 so were excluded from the dataset, reducing sample size to n = 21 – 23. Overnight fasted glucose was measured at 8 weeks of age. At 10 weeks of age, urine was collected by scruffing the mouse over a microtube, if the mouse did not spontaneously urinate, this was encouraged by gently stroking the abdomen. At 12 weeks of age, indirect calorimetry was carried out using in PhenoMaster metabolic cages (TSE systems, Bad Homburg, Germany) for 48 h on a subset of mice (n = 16 – 19, see section 2.3 for details). Mice were then transferred to light controlled cabinets, where they remained group housed, and half of the mice underwent an advancement of light onset by 7 h so that there were now four groups of mice (*Zfhx3*$^{Sci/+}$ and *Zfhx3*$^{+/+}$, lights on 0700 and lights on 2400; n = 11 - 13). The mice were allowed to acclimate to the new 12 h : 12 h light : dark schedule for 14 days before they were humanely killed by cervical dislocation at ZT 3 or ZT 15 and the brain was collected and frozen on dry ice for storage at -70 ˚C.

2.2 Enzyme – Linked Immunosorbent Assays (ELISAs)

Leptin (Invitrogen, cat no KMC2281), insulin-like growth factor-1 (IGF1; R & D systems, cat no MG100), and insulin (Mercodia, cat no 10-1247) were measured in serum samples from mice in *experiment 1*,

according to kit instructions. For the leptin ELISA, samples were diluted 1/10 and 1/20. Corticosterone was measured in urine collected from mice in *experiment 3* at ZT 1 and ZT 11, at either end of the light phase on the same day for each mouse. Only samples from mice with urine collected at both timepoints were measured (n = 15 – 16), according to kit instructions (Assaypro cat no EC3001-1) at a 1/20 dilution. For serum samples where measured values fell below the expected physiological range, and whose values were detected as potential outliers by Grubb's test ($P < 0.05$), these were excluded from the results (Leptin: one female *Zfhx3*$^{Sci/+}$, one male *Zfhx3*$^{+/+}$; IGF1: one male and one female *Zfhx3*$^{Sci/+}$, one female *Zfhx3*$^{+/+}$). For urine corticosterone samples, several ZT 11 samples exceeded the limit of the standard curve, and it was not possible to remeasure, so these values were artificially capped at the maximum for that assay at 104.98 ng / µl.

2.3 Indirect Calorimetry

Mice were individually housed in PhenoMaster cages for 3 days. The respiratory exchange ratio, energy expenditure and food and water consumption were recorded throughout this period. However, to allow mice to acclimatise to being introduced to a novel environment, analysis of metabolic parameters was performed upon only the final 24 hours of recording. Food and water were available *ad libitum* throughout testing.

2.4.1 Riboprobe synthesis

Riboprobes were previously synthesised for *Dio2, Dio3* [13], *Gpr50 [14], Sst, Ghrh* [15], *Npy* [16], *Pomc* [17], *Trhr1* [18]. For riboprobes not previously synthesised, a gene fragment 300-500 bp was synthesised with the following 5' and 3' overhangs containing M13 forward and reverse amplification sites and T3 and T7 polymerase sites respectively to facilitate amplification: 5'-GATTCGGAAACAGCTATGACCATGATTACGCCAAGCGCGCAATTAACCCTCACTAAAGGGAACAAAAGCTGG GTACC-3', 5'-GAGCTCCAATTCGCCCTATAGTGAGTCGTATTACGCGCGCTCACTGGCCGTCGTTTTACAATT-3' (gblock, IDT). New riboprobes were produced for *Bmal1* (accession no. NM_007489.4, range: 1389 – 1882)*, Dlk1* (accession no. NM_010052.5, range: 337 – 610)*, Ghr* (accession no. NM_010284.3, range: 1066 – 1556)*, Otp* (accession no. NM_011021.5, range: 135 – 691)*, Sim1* (accession no. U40575.1, range: 247 – 546)*, Tbx3* (accession no. NM_011535.3 range: 1648 – 1963)*,* and *Trh* (accession no. NM_009426.3, range: 114 – 463). Gene fragments were amplified by polymerase chain reaction amplification with M13 forward and reverse primers, which amplified 5' upstream of polymerase sites. 100 ng of PCR product was used in an *in vitro* transcription reaction with T7 polymerase (antisense) in the presence of ^{35}S-uridine 5 triphosphate (Perkin Elmer) for radioactive *in situ* hybridisation. Sense probes were also produced, using T3 polymerase, for use as a negative control when testing new antisense probes (suppl. figure 3).

2.4.2 *In situ* Hybridisation

Brains were cryosectioned on the coronal axis at 14 µm, mounted on poly – L – lysine coated slides (ThermoFisher) and stored at -70 ˚C. Radiolabelled i*n situ* hybridisation was performed as previously described [19]: slides were fixed in 4 % PFA – 0.1M phosphate buffer before acetylation in 0.25 % acetic anhydride – 0.1 M triethanolamine, pH 8 and then ^{35}S-labelled riboprobes (approx. 10^6 counts / minute / slide) were applied to slides in hybridization buffer containing 0.3 M NaCl, 10 mM Tris-HCl (pH 8), 1 mM EDTA, 0.05 % tRNA, 10 mM dithiothreitol, 0.02 % ficoll, 0.02% polyvinylpyrrolidone, 0.02% bovine serum albumin and 10% dextran sulphate and hybridized for 16 h at 58 ˚C. Slides were then washed in 4x saline sodium citrate (SSC; 1x SSC: 0.15 M NaCl, 15 mM sodium citrate), incubated with RNase A (20 µg / µl) at 37 ˚C and washed in decreasing concentrations of SSC to 0.1x at room temperature and in a final incubation in 0.1x SSC at 60 ˚C. Slides were then dehydrated and opposed to Biomax MR film (Kodak) for 1-21 days as appropriate.

2.6 Statistical Analysis

Statistical comparisons were carried out using GraphPad Prism v 9.0.0. Data are expressed throughout as mean ± SEM and individual values plotted where appropriate. Comparisons were by unpaired t-test or 2-way ANOVA with Šídák's multiple comparisons test. This was also carried out for continuous data when both sexes and genotypes were compared, with multiple 2-way ANOVAs being carried out to allow for pairwise comparisons within timepoints. For continuous data that only considered one sex, a 2-way repeated measures ANOVA was carried out followed by Šídák's multiple comparisons test. For indirect calorimetry, 24 h, light phase and dark phase data were compared by lean mass-adjusted ANCOVA as recommended in [20], using quantitative NMR lean mass from 1 – 2 days before entering the phenomaster cages. When data did not meet the assumptions of the test, it was transformed and the analysis carried out on transformed data (*Sim1, Npy, Dio2;* log transformed), or non-parametric tests (Mann-Whitney and / or Wilcoxon matched-pairs signed rank) were used where appropriate and indicated in the text.

3. Results

3.1 *Zfhx3*$^{Sci/+}$ mice are smaller and leaner than wildtype littermates

We first examined whole animal metabolic phenotypes in 12-month-old male and female *Zfhx3*$^{Sci/+}$ mice (*experiment 1*). The *Sci* mutation led to a lower body weight in both male and female mice (Figure 1 A, P < 0.0001), and nose-base of tail length was significantly reduced in female mice and in *Zfhx3*$^{Sci/+}$ mice, with those harbouring the *Sci* mutation having 0.87 ± 0.05 cm (8.27 ± 0.47 %) shorter body length than wildtype (Figure 1 B, Genotype: P < 0.0001, Sex: P = 0.0499, within sex both P < 0.0001). This was accompanied by lower lean mass in *Zfhx3*$^{Sci/+}$ mice and female mice overall (Figure 1 C, Genotype: P < 0.0001, Sex: P < 0.0001, within sex both P < 0.0001), the same effect was seen for fat mass (Figure 1 E, Genotype: P = 0.0008, Sex: P < 0.0001, within female P = 0.0187), but when corrected to body mass, lean mass % and fat mass % only differed by sex overall (Figures 1 D, F; sex both: P < 0.0001). On comparison of fat depot mass (Figure 1 G – K), only mesenteric adipose tissue differed by genotype, with an overall reduction in *Zfhx3*$^{Sci/+}$ mice (P = 0.0051), and interscapular brown adipose tissue approached a significantly lower mass in *Zfhx3*$^{Sci/+}$ mice overall (P = 0.0535). However, when corrected for body weight, no effect of the *Sci* mutation was detected in any of the adipose depots measured (supplemental figure 1), so according to these measurements the adipose depots were proportionate to body weight in these smaller mice.

3.2 *Zfhx3*$^{Sci/+}$ mice have lower circulating anabolic hormone concentrations

Comparison of fasted serum leptin revealed lower circulating levels overall in *Zfhx3*$^{Sci/+}$ and female mice, with the genotype effect being stronger in the female values (Figure 2 A: Sex P < 0.0001, Genotype P = 0.0067, Sex x Genotype P = 0.0214, within female P = 0.0029), and when normalised to fat mass, only the sex difference remained (Figure 2 B; P < 0.0001), demonstrating that genotype effects on circulating leptin were likely a reflection of reduced adiposity in the *Zfhx3*$^{Sci/+}$ mice. Fasted insulin was reduced in *Zfhx3*$^{Sci/+}$ mice (Figure 2 C, P = 0.0014), suggesting a protective metabolic effect of the *Sci* mutation. Circulating IGF1 was also lower in *Zfhx3*$^{Sci/+}$ mice (Figure 2 D, Genotype: P = 0.0004, Sex: P = 0.0152, within male P = 0.0118), implying, together with whole body mass and length differences, a somatic growth inhibition associated with the *Sci* mutation in 12-month-old mice.

3.3 *Zfhx3*$^{Sci/+}$ mice consume less food than wildtype littermates

To determine if the *Sci* mutation reduced appetite, a cohort of male and female *Zfhx3*$^{Sci/+}$ and *Zfhx3*$^{+/+}$ mice were pair-housed in genotype and sex matched cages and their food and body weight measured on a weekly basis from 8 – 20 weeks of age (*experiment 2*). Body weight was collected for all mice up to 18 weeks. At the second week of measurement, at 10 weeks of age, already a reduced cumulative

food intake was detected in *Zfhx3*$^{Sci/+}$ mice, and this was maintained through the continuation of the experiment (Figure 3 A, P < 0.01 weeks 10 -20), with an expected higher food intake in male mice compared to females detected in these same weeks (P < 0.001 weeks 10-20). Within-sex genotype differences were detected for several of these weeks for both male and female mice (weeks 10 – 14, 20 female, weeks 11 – 15, 20, male), with differences approaching significance for weeks 15 – 19 in female and 16 – 19 in male mice. Surprisingly, the *Zfhx3*$^{Sci/+}$ body weight differences at this younger age were more apparent in female mice. As expected, female mice weighed significantly less than males throughout the experiment (Figure 3 B, week 8 P = 0.0355, week 9 P = 0.0007, weeks 10 – 18 P < 0.0001). *Zfhx3*$^{Sci/+}$ mice weighed significantly less overall between weeks 9 – 13 (P < 0.05), and this difference approached significance for weeks 14 -18, however pairwise comparisons within female groups demonstrated a significantly lower body weight in *Zfhx3*$^{Sci/+}$ mice from 10 weeks old onwards (P < 0.05), with interaction between sex and genotype reaching significance at weeks 15 and 18.

3.4 Early differences in body weight are driven by lower lean mass gain by *Zfhx3*$^{Sci/+}$ female mice

To investigate more thoroughly early differences in weight gain, a cohort of *Zfhx3*$^{Sci/+}$ and *Zfhx3*$^{+/+}$ female mice were established, with the sample size established to humanely kill at two timepoints at the end of the experiment (*experiment 3*). Body weight, lean mass and fat mass were measured every two weeks from 6 – 14 weeks old. Body weight was lower in *Zfhx3*$^{Sci/+}$ mice (Figure 4 A, P = 0.0002), with an interaction between time and genotype (P = 0.0470), reaching significance in pairwise comparisons from week 10. Lean mass was significantly lower in *Zfhx3*$^{Sci/+}$ mice (Figure 4 B, P < 0.0001), and neither absolute fat mass, % fat mass differed by genotype (Figures 4 C, D). Fasted glucose did not differ in *Zfhx3*$^{Sci/+}$ mice at 8 weeks (Figure 4 E). As an indicator of peripheral and hormonal circadian rhythm, urinary corticosterone was measured at timepoints approaching its expected peak and nadir levels (Figure 4 F). As with *Zfhx3*$^{+/+}$ mice, *Zfhx3*$^{Sci/+}$ mice had significantly higher urinary corticosterone at ZT 11 (Wilcoxon matched-pairs rank test, *Zfhx3*$^{+/+}$ P = 0.0002, *Zfhx3*$^{Sci/+}$ P < 0.0001), and no genotype differences were detected (Mann Whitney, NSD). At 12 weeks of age, a subset of mice underwent indirect calorimetry. 24 h respiratory exchange ratio (RER) approached significantly lower levels in *Zfhx3*$^{Sci/+}$ mice (Figure 4 G, I: genotype P = 0.0546; time x genotype P = 0.0048. RER was lower in *Zfhx3*$^{Sci/+}$ mice when only the dark (active) phase was considered (P = 0.0306). There was a significant reduction in *Zfhx3*$^{Sci/+}$ mice energy expenditure (time course, P = 0.0037), and an interaction between time and genotype (P < 0.0001), illustrated by significantly lower energy expenditure in *Zfhx3*$^{Sci/+}$ mice in only the first 7 h of the dark (active) phase (Figure 4 H). This was confirmed when corrected for lean mass by ANCOVA, energy expenditure was significantly lower in *Zfhx3*$^{Sci/+}$ mice during the dark phase (P = 0.0239), and total and light phase reductions approached significance (Figure 4 J). Food and water intake were measured during indirect calorimetry, and no genotype effect was detected in food intake over 24 h sample time (supplementary figure 2 A, B). However, a significant reduction in water intake was detected in *Zfhx3*$^{Sci/+}$ mice, (supplementary figure 2 C, D; Genotype P = 0.0125, Time x Genotype P = 0.0013; dark phase only P = 0.0020).

3.5 Hypothalamic mRNA expression is altered in female *Zfhx3*$^{Sci/+}$ mice

Candidate genes were investigated for altered expression in female *Zfhx3*$^{Sci/+}$ mice in brains collected at ZT 3 in the light phase and ZT 15 in the dark phase. Genes were chosen based on previous observations as well as those associated with growth and energy balance in the hypothalamus. Table 1 summarises the genes investigated and where expression was detected. *Npy, Pomc, Sim1, Sst, Tbx3,* and *Trh* transcripts that had previously been implicated as altered by the *Sci* mutation in a previous RNA-seq experiment [10] were not detected in the SCN, indicating that expression of these transcripts may be altered in other hypothalamic nuclei.

3.5.1. Hypothalamic growth axis component expression is altered in the arcuate nucleus

Radioactive *in situ* hybridisation was used to quantify spatially distinct expression of hypothalamic growth axis components. Expression of growth hormone-releasing hormone (*Ghrh*), the stimulatory arm of the growth axis, was decreased in the arcuate nucleus (ARC) of *Zfhx3*$^{Sci/+}$ mice (Figure 5 A, P = 0.0088), with pairwise comparisons reaching significance in the dark phase (ZT 15, P = 0.0405). In the inhibitory arm of the growth axis, somatostatin (*Sst*) mRNA expression was increased in the ARC of *Zfhx3*$^{Sci/+}$ mice (Figure 5 B, P = 0.0089), and ARC growth hormone-receptor (*Ghr*) expression was reduced overall in *Zfhx3*$^{Sci/+}$ mice and with significantly increased overall expression at ZT 15 (Figure 5 C, Genotype P = 0.0333, ZT P = 0.0107). Interestingly, no differences in expression were detected in these genes in the more anterior hypothalamic nuclei (Figure 5 D: *Ghrh,* posterior hypothalamus (PoPVN), E: *Sst,* periventricular nucleus (PeVN), F: *Ghr,* paraventricular nucleus (PVN).

3.5.2 Additional candidate hypothalamic gene expression altered by the *Sci* mutation

We measured expression of the circadian gene *Bmal1* as an indicator of rhythmic gene expression in the suprachiasmatic nucleus (SCN). Overall, there was a significantly higher *Bmal1* expression in the dark phase (Figure 6 A, P = 0.0008), and an interaction between ZT and genotype (P = 0.0052). Multiple comparisons indicated increased *Bmal1* expression in the dark phase only for *Zfhx3*$^{+/+}$ mice (P = 0.0002) and lower expression in *Zfhx3*$^{Sci/+}$ mice at ZT 15 (P = 0.0445). This may indicate dysregulation of *Bmal1* circadian expression. Expression of appetite suppressing peptide *Pomc* approached a significant reduction in the ARC of *Zfhx3*$^{Sci/+}$ mice (Figure 6 B, P = 0.0607) and appetite stimulating peptide *Npy* was significantly reduced overall in *Zfhx3*$^{Sci/+}$ mice, with a significantly lower expression in *Zfhx3*$^{Sci/+}$ mice at ZT 15 (Figure 6 C, Genotype P = 0.0294, within ZT 15 P = 0.0365). Expression of *Gpr50* in the ventricular ependymal layer was overall increased in *Zfhx3*$^{Sci/+}$ mice, reaching significance in pairwise comparisons at ZT 15 (Figure 6 D, Genotype P = 0.0188, within ZT 15 P = 0.0325). Further genes investigated for altered expression did not differ with genotype (supplementary figure 4). Expression of *Otp* in the paraventricular nucleus (PVN) was reduced overall at ZT 3 (suppl. figure 4 A, P = 0.0015), and expression of ventricular ependymal layer *Dio2* was increased at ZT 15 (suppl. figure 4 D, P = 0.0285) as was dorsomedial hypothalamus (DMH) *Trh* (suppl. figure 4 F, P = 0.0145). Expression of PVN *Sim1, Trh,* ARC *Trh-r1, Dlk1* and *Tbx3* did not differ by genotype or ZT (suppl. figure 4).

4. Discussion

This study establishes a lean and metabolically protective phenotype in *Zfxh3*$^{Sci/+}$ mice aged to 12 months old, likely a progressive effect of inhibited growth and appetite over their lifespan, with younger mice demonstrating a slower increase in lean mass from the earliest measured timepoint at 6 weeks of age. This was accompanied by altered hypothalamic gene expression in growth and appetite regulating peptide mRNAs in the ARC. In particular, *Sst* and *Gpr50* contain the AT motif that ZFHX3 can bind to alter expression, and therefore likely drive the observed protective metabolic phenotype.

Many studies in humans and model rodents have demonstrated a link between disrupted circadian rhythm and body weight regulation [21], and growth axis component IGF1 has even been implicated in entrainment of circadian rhythm through food intake [22]. It is key to note that despite building evidence for the role of ZFHX3 in regulating circadian phenotype, in the present study mice did not undergo any circadian challenge. ZHFX3 transcriptionally regulates key SCN coordinators of clock function *Vip* and *Avp* through the same AT motif contained in the promoters of *Sst* and *Gpr50.* Notably, previously detected mis-regulated hypothalamic transcripts include additional neuropeptides and their receptors. So it is entirely likely that the same mechanisms drive disruption of multiple transcripts in the ARC.

Importantly, Parsons *et al.* demonstrated that disrupted core clock gene expression in the SCN of *Zfhx3*$^{Sci/+}$ mice was masked in LD 12:12 conditions [10]. Interestingly, SCN *Bmal1* rhythm did appear altered in *Zfhx3*$^{Sci/+}$ mice, being higher in the light phase and lower in the dark phase compared to wildtype littermates. The limitation of only sampling two timepoints means that it is not clear whether this is an overall damping of *Bmal1* rhythm in the SCN, a global reduction independent of circadian phase, or a shift in the rhythm of this core clock gene. In the present study we found that female mice had an intact peak and trough in urinary corticosterone levels, suggesting that peripheral rhythms remained unaltered by the *Sci* mutation. Given the known peripheral clock synchronising effect of corticosterone [23], the implication is that peripheral rhythms remained intact and did not drive metabolic effects in these mice. Indeed, mRNA expression of transcripts outside of the SCN: *Trh, Otp, Dio2* and *Ghr* did differ in expression with respect to the time of day and independent of genotype, supporting intact peripheral circadian rhythms. Therefore it is likely that the metabolic effects detected in the present study were independent of the circadian actions of ZFHX3 and support a hypothesis that pleiotropy associated with this mutation affects numerous neuropeptide regulatory mechanisms in the hypothalamus.

In the present study we demonstrate that both male and female *Zfxh3*$^{Sci/+}$ mice weigh less and have reduced adiposity at 1 year . Although reduced fat mass, including specifically the visceral mesenteric fat depot, could be accounted for by smaller body size, and lower circulating fasted leptin was in proportion to fat mass, these mice ate less and had a lower fasted insulin level. Notably, the present study identified low circulating IGF1 in *Zfxh3*$^{Sci/+}$ mice, an indicator of growth axis suppression. IGF1 null mice have low viability and are born small, with inhibited growth [24]. Moreover, liver specific deletion of IGF1 leads to elevated levels of growth hormone and this is presumed to contribute to the insulin resistance but not elevated blood glucose they experience [25]. Since it was not possible to measure growth hormone in the present study, it is assumed that reduced IGF1 was a consequence of lowered growth axis tone, likely driven from the altered gene expression in the hypothalamus, and not a direct effect of the *Zfhx3*^{Sci} mutation, however this cannot be discounted. The reduced somatic growth effect was demonstrated in female mice from 6 weeks of age, when we already detected lower lean and whole body mass. It is tempting to extrapolate from this data that a fat mass gain was starting to wane for *Zfxh3*$^{Sci/+}$ mice at 16 weeks, leading to the fat mass differences seen in the aged mice, but these measurements were not possible given the constraints of the experimental plan.

When considering changes in growth axis component gene expression in the hypothalamus of *Zfxh3*$^{Sci/+}$ mice, it was perhaps unsurprising that expression was altered only in the ARC, where *Zfhx3* is demonstrably expressed [11], with the inhibitory arm (somatostatin) upregulated and the stimulatory arm (GHRH) downregulated. Classically, it has been shown that the *Sst* neurons in the ARC predominantly project within the ARC to *Ghrh* neurons [26,27], which then project to the median eminence and release GHRH to somatotrophs of the anterior pituitary to alter growth hormone secretion [28]. More recent work in human tissue supports active synapses from SST to GHRH neurons within the ARC [29]. Thus, although we cannot rule out direct regulation by ZFHX3 of GHRH, it is the most parsimonious explanation that altered ZFHX3 binding to the *Sst* AT motif in *Zfxh3*$^{Sci/+}$ mice leads to upregulation of somatostatin, with subsequent inhibition of *Ghrh* production and suppression of the growth axis. We have previously demonstrated that somatostatin analogues inhibit somatic growth and circulating IGF1 in Siberian hamsters (*Phodopus sungorus*) [30,31], driving changes in body weight and fasting glucose and insulin as well as increased incidence of daily torpor [32].

We found suppressed food intake in both male and female *Zfxh3*$^{Sci/+}$ mice from 10 weeks old, and detected decreased expression of appetite stimulating peptide *Npy* mRNA in 14 week old female mice. Links between NPY and the growth axis are well established, stimulating GHRH and suppressing somatostatin release from PeVN neurons to the hypophyseal blood portal system to reach pituitary

somatotrophs in sheep [33,34], and genetically altered mice [35]. In broiler chickens, treatment with growth hormone decreases NPY levels [36], and *npy* expression is reduced in zebrafish (*Danio rerio*) overexpressing growth hormone [37]. Intracerebroventricular injection of NPY decreases plasma growth hormone in rats, postulated to be via stimulation of somatostatin neurons [38,39]. However following hypophysectomy, low *Npy* expression in the ARC can be rescued, and stimulation of *C-fos* is seen in NPY neurons of the ARC with chronic treatment with growth hormone [40,41]. Due to the lack of known ZHFX3-binding motifs in *Npy*, it is not clear whether the *Sci* mutation directly alters expression of this gene, whether altered expression is a downstream effect of the suppressed somatic growth axis, or via some other mechanism.

In the present study we found that energy expenditure was lower in *Zfxh3*$^{Sci/+}$ mice, particularly in the dark phase when mice are usually more active. We measured higher expression of *Gpr50* mRNA in the ventricular ependymal layer of the hypothalamus in *Zfxh3*$^{Sci/+}$ mice. The mouse *Gpr50* promotor contains an AT motif that ZFHX3 may bind to alter expression [10]. This orphan G protein-coupled receptor is implicated in regulation of energy expenditure; mice lacking *Gpr50* weigh less and are protected from diet induced obesity, likely due to increased energy expenditure [42]. It is therefore possible that increased expression of *Gpr50* contributed to the lower energy expenditure seen in *Zfxh3*$^{Sci/+}$ mice.

The use of GWAS to identify genetic drivers of obesity and therefore potential targets for intervention can be controversial, as the majority of common variants are located in non-coding regions of the genome and thus present significant challenges to investigation and interpretation. The first time ZFHX3 was associated with human body weight was when a rare protein altering variant was identified in a human population of predominantly European ancestry [7]. This Q2021H variant is in a similarly highly conserved region to the *Sci* mutation and knockout of the *Drosophila* homologue (*zfh2*) led to increased whole body triglycerides, which the authors interpreted as increased adiposity, whether knocked down in neural or adipose tissue in the flies. Considering the metabolic phenotype described in the present study, it is tempting to hypothesise that the low frequency human Q2021H ZFHX3 variant, present in 4.34 % of sampled populations, might act through a similar pathway to that seen in the V1963F *Sci* mouse mutation.

5. Conclusion

We have demonstrated a protective metabolic phenotype in *Zfxh3*$^{Sci/+}$ mice and associated altered hypothalamic gene expression; notably in ARC growth axis components, *Npy* and *Gpr50*. This supports a pleiotropic role for ZFHX3 in regulation of bodyweight, appetite and energy expenditure through these central pathways, and may explain the association with BMI in humans.

Appendices

Supplementary figures are provided in a separate file.

Declaration of Interest

The authors declare no conflict of interest.

Acknowledgements

The authors thank the staff of the Mary Lyon Centre and core services at MRC Harwell Institute for assistance with mouse studies. PMN was supported by the Medical Research Council (MC_U142684173), the Barrett lab was supported by the Scottish Government, R. Dumbell was supported by the Medical Research Council (Roger Cox: MC_U142661184), Nottingham Trent University and a Research Visit Grant from the British Society for Neuroendocrinology to carry out this work.

Author Contributions

RD, PMN, NB and PB contributed to conceptualisation of the project; mouse colony management was carried out by RH and LK; experiments and sample collection were performed by RD, GB, AGW, LB, LM, LK and DW; the original draft was written by RD and reviewed and edited by RD, PMN, GB and PB, with support from all authors.

References

[1] Di Angelantonio, E., Bhupathiraju, S.N., Wormser, D., Gao, P., Kaptoge, S., de Gonzalez, A.B., et al., 2016. Body-mass index and all-cause mortality: individual-participant-data meta-analysis of 239 prospective studies in four continents. Lancet 388:776-786.

[2] Stefan, N., Birkenfeld, A.L., Schulze, M.B., Ludwig, D.S., 2020. Obesity and impaired metabolic health in patients with COVID-19. Nature reviews.Endocrinology 16:341-342.

[3] Elks, C.E., den Hoed, M., Zhao, J.H., Sharp, S.J., Wareham, N.J., Loos, R.J.F., et al., 2012. Variability in the heritability of body mass index: a systematic review and meta-regression. Frontiers in endocrinology (Lausanne) 3:29.

[4] Locke, A.E., Kahali, B., Berndt, S.I., Justice, A.E., Pers, T.H., Day, F.R., et al., 2015. Genetic studies of body mass index yield new insights for obesity biology. Nature 518:197-206.

[5] Akiyama, M., Okada, Y., Kanai, M., Takahashi, A., Momozawa, Y., Ikeda, M., et al., 2017. Genome-wide association study identifies 112 new loci for body mass index in the Japanese population. Nat Genet 49:1458-1467.

[6] Schwartz, M.W., Woods, S.C., Porte Jr, D., Seeley, R.J., Baskin, D.G., 2000. Central nervous system control of food intake. Nature 404:661-671.

[7] Turcot, V., Lu, Y., Highland, H.M., Schurmann, C., Justice, A.E., Fine, R.S., et al., 2018. Protein-altering variants associated with body mass index implicate pathways that control energy intake and expenditure in obesity. Nat Genet 50:26-41.

[8] Morinaga, T., Yasuda, H., Hashimoto, T., Higashio, K., Tamaoki, T., 1991. A human alpha-fetoprotein enhancer-binding protein, ATBF1, contains four homeodomains and seventeen zinc fingers. Molecular and cellular biology 11:6041-6049.

[9] Yasuda, H., Mizuno, A., Tamaoki, T., Morinaga, T., 1994. ATBF1, a multiple-homeodomain zinc finger protein, selectively down-regulates AT-rich elements of the human alpha-fetoprotein gene. Molecular and cellular biology 14:1395-1401.

[10] Parsons, M.J., Brancaccio, M., Sethi, S., Maywood, E.S., Satija, R., Edwards, J.K., et al., 2015. The Regulatory Factor ZFHX3 Modifies Circadian Function in SCN via an AT Motif-Driven Axis. Cell 162:607-621.

[11] Lein, E.S., Hawrylycz, M.J., Ao, N., Ayres, M., Bensinger, A., Bernard, A., et al., 2007. Genome-wide atlas of gene expression in the adult mouse brain. Nature 445:168-176.

[12] Wilcox, A.G., Vizor, L., Parsons, M.J., Banks, G., Nolan, P.M., 2017. Inducible Knockout of Mouse Zfhx3 Emphasizes Its Key Role in Setting the Pace and Amplitude of the Adult Circadian Clock. J Biol Rhythms 32:433-443.

[13] Barrett, P., Ebling, F.J.P., Schuhler, S., Wilson, D., Ross, A.W., Warner, A., et al., 2007. Hypothalamic thyroid hormone catabolism acts as a gatekeeper for the seasonal control of body weight and reproduction. Endocrinology 148:3608-3617.

[14] Drew, J.E., Barrett, P., Mercer, J.G., Moar, K.M., Canet, E., Delagrange, P., et al., 2001. Localization of the melatonin-related receptor in the rodent brain and peripheral tissues. Journal of neuroendocrinology 13:453-458.

[15] Ross, A.W., Johnson, C.E., Bell, L.M., Reilly, L., Duncan, J.S., Barrett, P., et al., 2009. Divergent Regulation of Hypothalamic Neuropeptide Y and Agouti-Related Protein by Photoperiod in F344 rats With Differential Food Intake and Growth. Journal of neuroendocrinology 21:610-619.

[16] Mercer, J.G., Bruce Lawrence, C., Moar, K.M., Atkinson, T., Barrett, P., 1997. Short-day weight loss and effect of food deprivation on hypothalamic NPY and CRF mRNA in Djungarian hamsters. American Journal of Physiology - Regulatory Integrative and Comparative Physiology 273:R768-R776.

[17] Mercer, J.G., Moar, K.M., Ross, A.W., Hoggard, N., Morgan, P.J., 2000. Photoperiod regulates arcuate nucleus POMC, AGRP, and leptin receptor mRNA in Siberian hamster hypothalamus. American Journal of Physiology - Regulatory Integrative and Comparative Physiology 278:R271-R281.

[18] Ebling, F.J.P., Wilson, D., Wood, J., Hughes, D., Mercer, J.G., Morgan, P.J., et al., 2008. The thyrotropin-releasing hormone secretory system in the hypothalamus of the siberian hamster in long and short photoperiods. Journal of neuroendocrinology 20:576-586.

[19] Morgan, P.J., Webster, C.A., Mercer, J.G., Ross, A.W., Hazlerigg, D.G., Maclean, A., et al., 1996. The ovine pars tuberalis secretes a factor(s) that regulates gene expression in both lactotropic and nonlactotropic pituitary cells. Endocrinology 137:4018-4026.

[20] McMurray, F., Church, C.D., Larder, R., Nicholson, G., Wells, S., Teboul, L., et al., 2013. Adult Onset Global Loss of the Fto Gene Alters Body Composition and Metabolism in the Mouse. PLOS Genetics 9:e1003166.

[21] Panda, S., 2016. Circadian physiology of metabolism. Science (American Association for the Advancement of Science) 354:1008-1015.

[22] Crosby, P., Hamnett, R., Putker, M., Hoyle, N.P., Reed, M., Karam, C.J., et al., 2019. PMC6506277; Insulin/IGF-1 Drives PERIOD Synthesis to Entrain Circadian Rhythms with Feeding Time. Cell 177:896-909.e20.

[23] Balsalobre, A., Brown, S.A., Marcacci, L., Tronche, F., Kellendonk, C., Reichardt, H.M., et al., 2000. Resetting of circadian time in peripheral tissues by glucocorticoid signaling. Science 289:2344-2347.

[24] Baker, J., Liu, J., Robertson, E.J., Efstratiadis, A., 1993. Role of insulin-like growth factors in embryonic and postnatal growth. Cell 75:73-82.

[25] Yakar, S., Liu, J.L., Fernandez, A.M., Wu, Y., Schally, A.V., Frystyk, J., et al., 2001. Liver-Specific igf-1 Gene Deletion Leads to Muscle Insulin Insensitivity. Diabetes (New York, N.Y.) 50:1110-1118.

[26] Ishikawa, K., Taniguchi, Y., Kurosumi, K., Suzuki, M., Shinoda, M., 1987. Immunohistochemical identification of somatostatin-containing neurons projecting to the median eminence of the rat. Endocrinology 121:94-97.

[27] Willoughby, J.O., Martin, J.B., 1978. Pulsatile growth hormone secretion: Inhibitory role of medial preoptic area. Brain research 148:240-244.

[28] Sawchenko, P.E., Swanson, L.W., Rivier, J., Vale, W.W., 1985. The distribution of growth-hormone-releasing factor (GRF) immunoreactivity in the central nervous system of the rat: An immunohistochemical study using antisera directed against rat hypothalamic GRF. Journal of Comparative Neurology 237:100-115.

[29] Proudan, N., Peroski, M., Grignol, G., Merchenthaler, I., Dudas, B., 2015. Juxtapositions between the somatostatinergic and growth hormone-releasing hormone (GHRH) neurons in the human hypothalamus. Neuroscience 297:205-210.

[30] Dumbell, R., Petri, I., Scherbarth, F., Diedrich, V., Schmid, H.A., Steinlechner, S., et al., 2017. Somatostatin Agonist Pasireotide Inhibits Exercise-Stimulated Growth in the Male Siberian Hamster (Phodopus sungorus). J Neuroendocrinol 29.

[31] Dumbell, R.A., Scherbarth, F., Diedrich, V., Schmid, H.A., Steinlechner, S., Barrett, P., 2015. Somatostatin Agonist Pasireotide Promotes a Physiological State Resembling Short-Day Acclimation in the Photoperiodic Male Siberian Hamster (Phodopus sungorus). J Neuroendocrinol 27:588-599.

[32] Scherbarth, F., Diedrich, V., Dumbell, R.A., Schmid, H.A., Steinlechner, S., Barrett, P., 2015. Somatostatin receptor activation is involved in the control of daily torpor in a seasonal mammal. Am J Physiol Regul Integr Comp Physiol 309:668.

[33] Morrison, C.D., Daniel, J.A., Hampton, J.H., Buff, P.R., McShane, T.M., Thomas, M.G., et al., 2003. Luteinizing hormone and growth hormone secretion in ewes infused intracerebroventricularly with neuropeptide Y. Domestic animal endocrinology 24:69-80.

[34] Gładysz, A., Krejci, P., Simůnek, J., Polkowska, J., 2001. Effects of central infusions of neuropeptide Y on the somatotropic axis in sheep fed on two levels of protein. Acta neurobiologiae experimentalis 61:255-266.

[35] Huang, L., Tan, H.Y., Fogarty, M.J., Andrews, Z.B., Veldhuis, J.D., Herzog, H., et al., 2014. Actions of NPY, and Its Y1 and Y2 Receptors on Pulsatile Growth Hormone Secretion during the Fed and Fasted State. The Journal of neuroscience 34:16309-16319.

[36] Wang, X., Day, Zhou, Y., Beard, J., Vasilatos-Younken, R., 2000. Evidence of a role for neuropeptide Y and monoamines in mediating the appetite-suppressive effect of GH. Journal of endocrinology 166:621-630.

[37] Dalmolin, C., Almeida, D., Figueiredo, M., Marins, L., 2015. Food intake and appetite control in a GH-transgenic zebrafish. Fish physiology and biochemistry 41:1131-1141.

[38] Rettori, V., Milenkovic, L., Aguila, M.C., McCann, S.M., 1990. Physiologically significant effect of neuropeptide Y to suppress growth hormone release by stimulating somatostatin discharge. Endocrinology 126:2296-2301.

[39] Pierroz, D.D., Catzeflis, C., Aebi, A.C., Rivier, J.E., Aubert, M.L., 1996. Chronic Administration of Neuropeptide Y into the Lateral Ventricle Inhibits Both the Pituitary-Testicular Axis and Growth Hormone and Insulin-Like Growth Factor I Secretion in Intact Adult Male Rats. Endocrinology 137:3-12.

[40] Kamegai, J., Minami, S., Sugihara, H., Higuchi, H., Wakabayashi, I., 1994. Growth hormone induces expression of the c-fos gene on hypothalamic neuropeptide-Y and somatostatin neurons in hypophysectomized rats. Endocrinology 135:2765-2771.

[41] Minami, S., Kamegai, J., Sugihara, H., Suzuki, N., Wakabayashi, I., 1998. Growth hormone inhibits its own secretion by acting on the hypothalamus through its receptors on neuropeptide Y neurons in the arcuate nucleus and somatostatin neurons in the periventricular nucleus. Endocrine journal 45:S19-S26.

[42] Ivanova, E.A., Bechtold, D.A., Dupre, S.M., Brennand, J., Barrett, P., Luckman, S.M., et al., 2008. Altered metabolism in the melatonin-related receptor (GPR50) knockout mouse. American Journal of Physiology - Endocrinology And Metabolism 294:176-182.

Figures

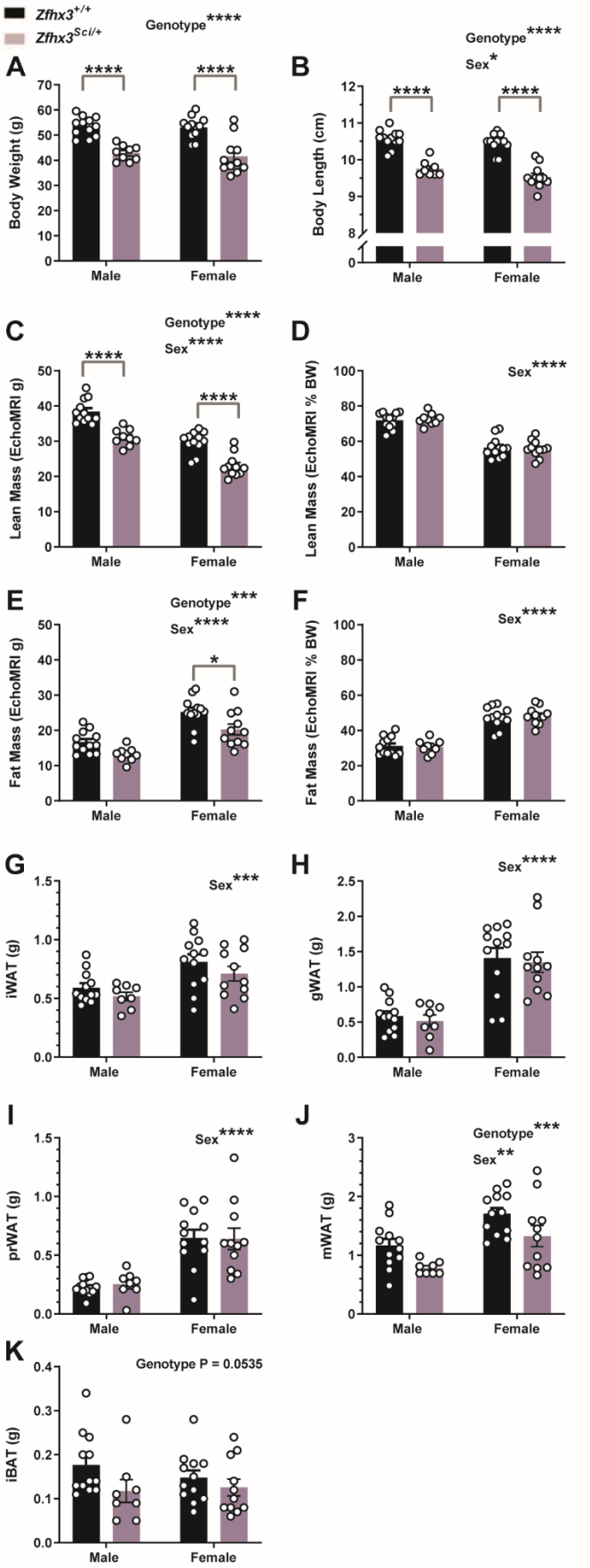

Figure 1.

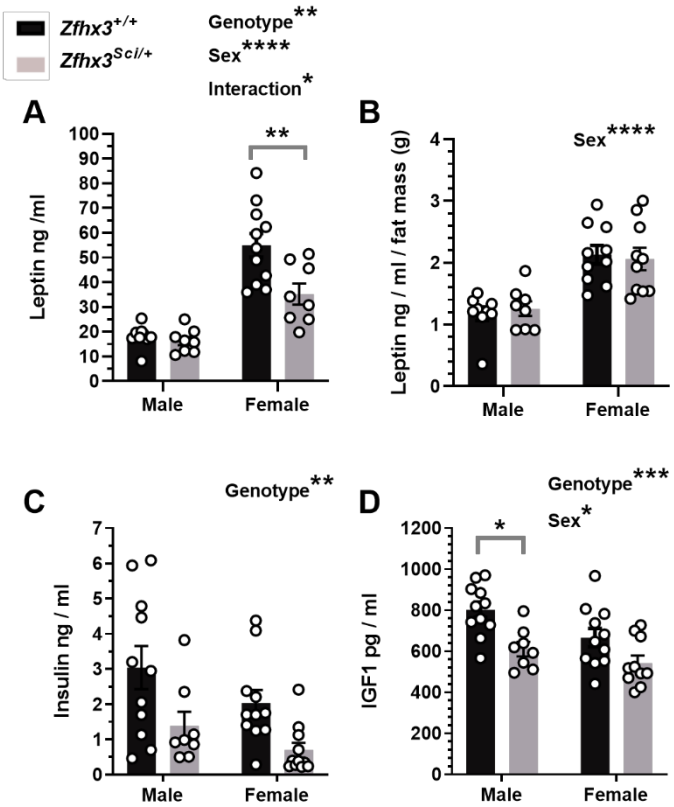
Zfhx3+/+
Zfhx3Scl/+
Genotype**
Sex****
Interaction*
A
Leptin ng /ml
**
Male
Female
B
Leptin ng / ml / fat mass (g)
Sex****
Male
Female
C
Genotype**
Insulin ng / ml
Male
Female
D
Genotype***
Sex*
IGF1 pg / ml
*
Male
Female

Figure 2.

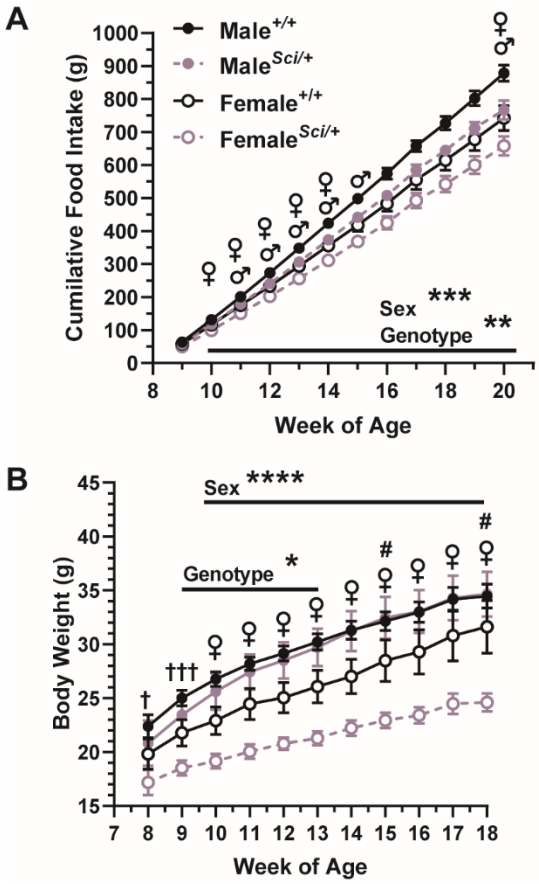
A
Male+/+
MaleSci/+
Female+/+
FemaleSci/+
Cumulative Food Intake (g)
Week of Age
Sex ***
Genotype **
B
Body Weight (g)
Week of Age
Sex ****
Genotype *

Figure 3.

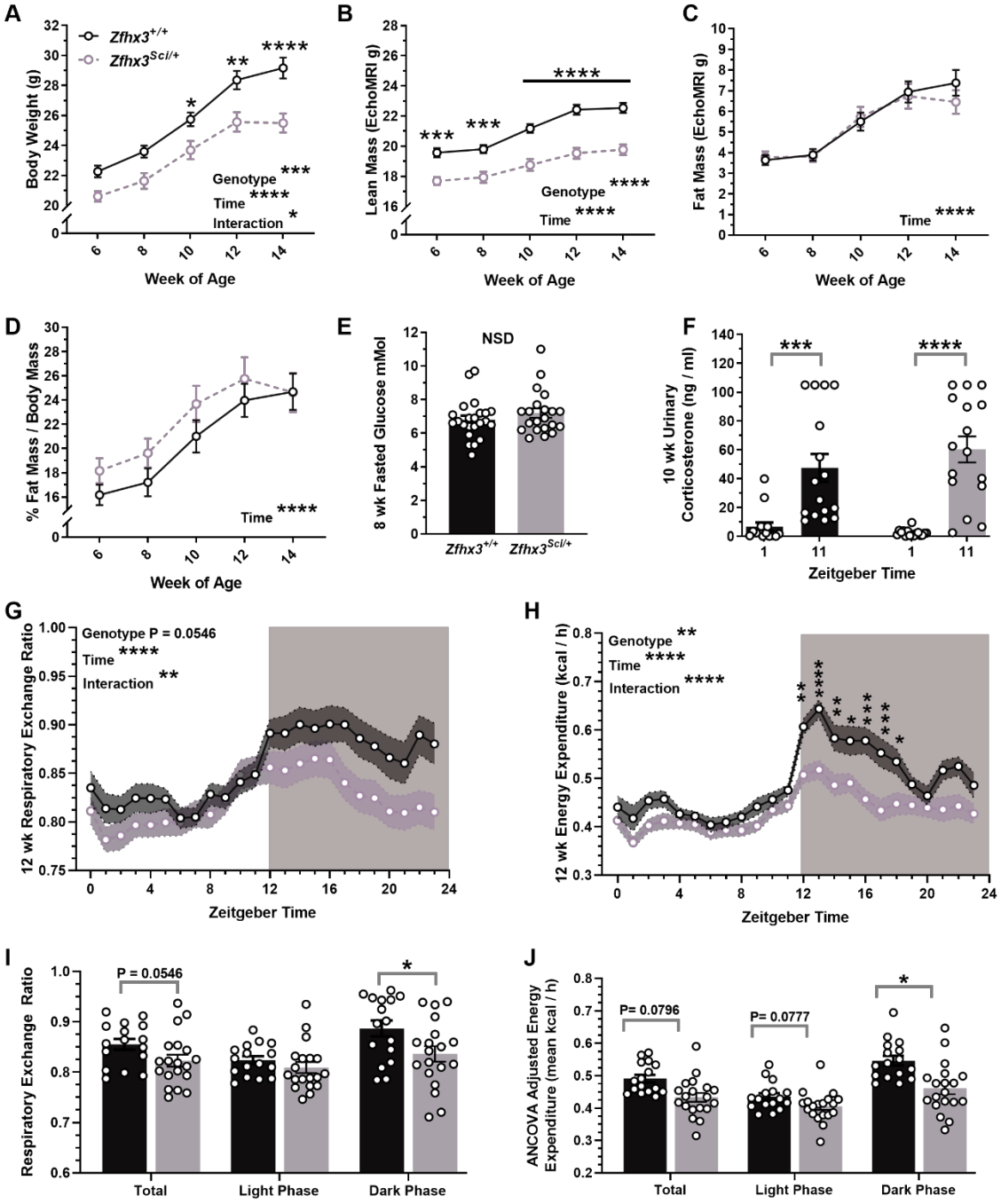
A
Zfhx3+/+
Zfhx3Sci/+
Body Weight (g)
Week of Age
Genotype ***
Time ****
Interaction *
B
Lean Mass (EchoMRI g)
Week of Age
Genotype ****
Time ****
C
Fat Mass (EchoMRI g)
Week of Age
Time ****
D
% Fat Mass / Body Mass
Week of Age
Time ****
E
8 wk Fasted Glucose mMol
NSD
Zfhx3+/+
Zfhx3Sci/+
F
10 wk Urinary Corticosterone (ng / ml)
Zeitgeber Time
G
12 wk Respiratory Exchange Ratio
Genotype P = 0.0546
Time ****
Interaction **
Zeitgeber Time
H
12 wk Energy Expenditure (kcal / h)
Genotype **
Time ****
Interaction ****
Zeitgeber Time
I
Respiratory Exchange Ratio
P = 0.0546
Total
Light Phase
Dark Phase
J
ANCOVA Adjusted Energy Expenditure (mean kcal / h)
P= 0.0796
P= 0.0777
Total
Light Phase
Dark Phase

Figure 4.

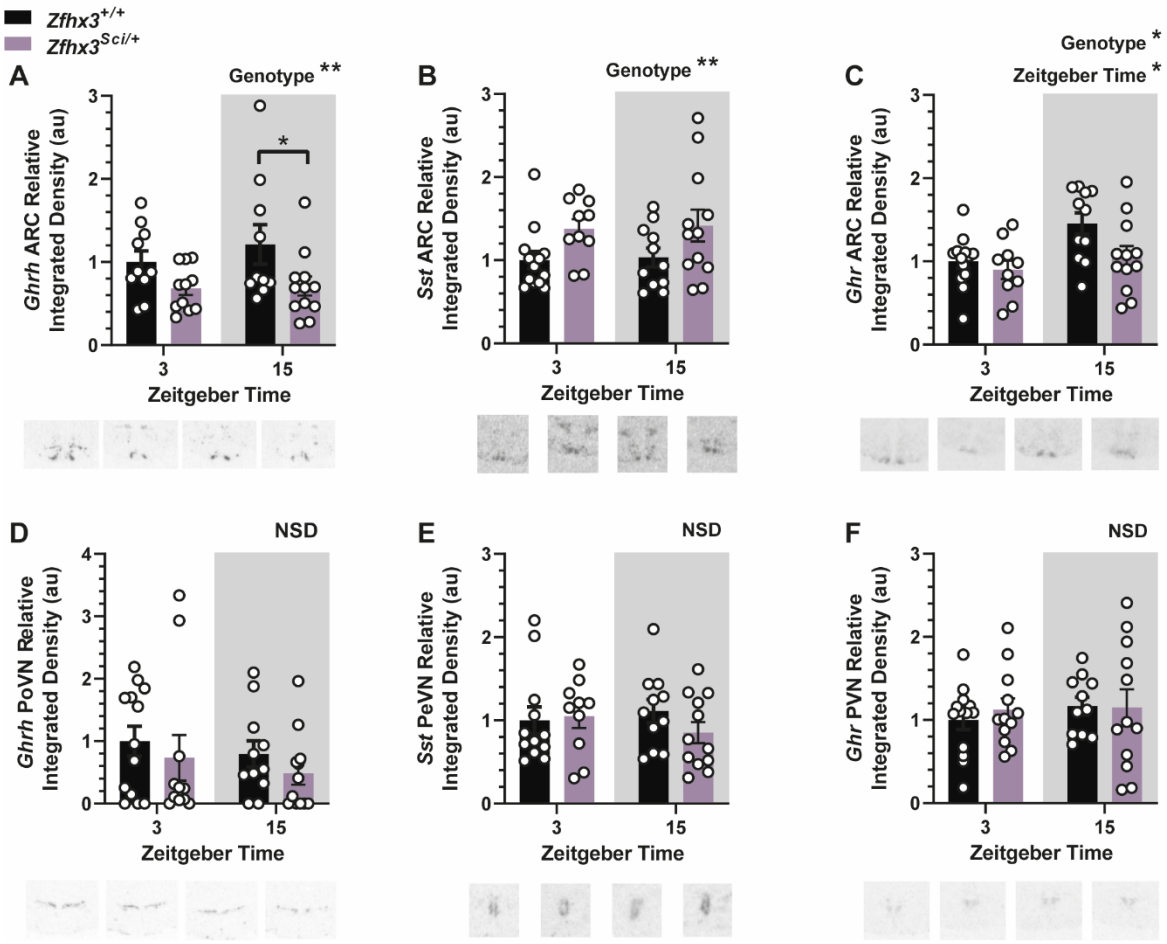
Zfhx3+/+
Zfhx3Sci/+
A
Genotype **
Ghrh ARC Relative Integrated Density (au)
Zeitgeber Time
B
Genotype **
Sst ARC Relative Integrated Density (au)
Zeitgeber Time
C
Genotype *
Zeitgeber Time *
Ghr ARC Relative Integrated Density (au)
Zeitgeber Time
D
NSD
Ghrh PoVN Relative Integrated Density (au)
Zeitgeber Time
E
NSD
Sst PeVN Relative Integrated Density (au)
Zeitgeber Time
F
NSD
Ghr PVN Relative Integrated Density (au)
Zeitgeber Time

Figure 5.

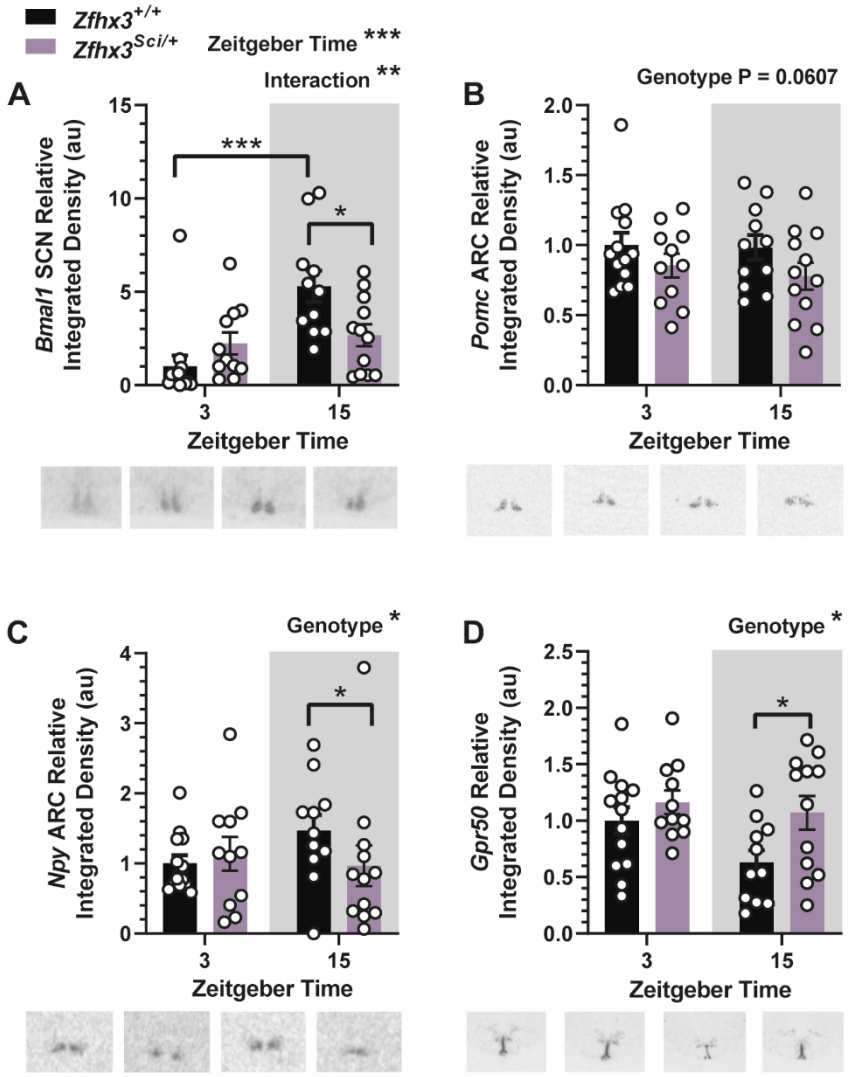
Zfhx3+/+
Zfhx3Sci/+
Zeitgeber Time ***
Interaction **
A
Bmal1 SCN Relative Integrated Density (au)
Zeitgeber Time
B
Genotype P = 0.0607
Pomc ARC Relative Integrated Density (au)
Zeitgeber Time
C
Genotype *
Npy ARC Relative Integrated Density (au)
Zeitgeber Time
D
Genotype *
Gpr50 Relative Integrated Density (au)
Zeitgeber Time

Figure 6.

Table 1.

Gene	Brain Region	mRNA detected?
Bmal1	SCN	+
Dio2	Ventricular ependymal layer	+
Dio3	Ventricular ependymal layer	-
Dlk1	ARC	+
Ghr	SCN	-
	PVN	+
	ARC	+
Ghrh	SCN	-
	PoPVN	+
	ARC	+
Gpr50	SCN	-
	Ventricular ependymal layer	+
Npy	SCN	-
	ARC	+
Otp	SCN	-
	PVN	+
Pomc	SCN	-
	ARC	+
Sim1	SCN	-
	PVN	+
Sst	SCN	-
	PeVN	+
	ARC	+
	SCN	-
Tbx3	ARC	+
Trh	SCN	-
	PVN	+
	DMH	+
Trhr1	ARC	+

Figure Legends

Figure 1: One year old *Zfhx3*$^{Sci/+}$ mice are smaller than wildtype littermates.
Male and female mice weigh less (A) and have shorter nose-tail body length (B) and lower lean (C) and fat mass (E) although this is proportionate to body weight (D, F). Fat depot weights at dissection did not differ by genotype, with the exception of mesenteric white adipose, which weighed less in *Zfhx3*$^{Sci/+}$ mice (G-K). Plotted are mean ± SEM with individual values. Statistical comparison is by 2-way ANOVA, with overall results and within-sex comparisons indicated on the graphs. ****P < 0.0001, *** P < 0.001, ** P < 0.01, * P < 0.05. BW: body weight, iWAT: inguinal white adipose tissue, gWAT: gonadal white adipose tissue, prWAT: perirenal white adipose tissue, mWAT: mesenteric white adipose tissue, iBAT: interscapular brown adipose tissue.

Figure 2: One year old *Zfhx3*$^{Sci/+}$ mice have lower circulating concentrations of metabolic hormones.
Circulating leptin was lower in fasted female *Zfhx3*$^{Sci/+}$ mice (A), however this is proportionate to fat mass (g, EchoMRI; B). Circulating insulin and insulin-like growth factor-1 (IGF1) were also lower in *Zfhx3*$^{Sci/+}$ mice. Plotted are mean ± SEM with individual values. Statistical comparison is by 2-way ANOVA, with overall results and within-sex comparisons indicated on the graphs. **** P < 0.0001, *** P < 0.001, ** P < 0.01, * P < 0.05.

Figure 3: Male and female *Zfhx3*$^{Sci/+}$ mice eat less than wildtype littermates.
Mice were pair-housed (genotype and sex matched) and food weighed weekly (A; n = 5-6 cages). Male mice ate more than female mice from the second week of the experiment, and *Zfhx3*$^{+/+}$ ate more than *Zfhx3*$^{Sci/+}$ mice from the second week of the experiment. The same mice were weighed weekly (B; n = 10-12), and the *Sci* mutation already inhibited weight gain from 9 weeks of age overall, with female *Zfhx3*$^{Sci/+}$ mice weighing less than wildtype littermates from 10 weeks old onwards. Although the genotype effect was not maintained from 14 weeks old onwards, a significant interaction could be detected at 15 and 18 weeks old. Plotted are mean ± SEM, statistical comparison is by 2-way ANOVA per timepoint, and within-sex differences are indicated on the graph. ♀ P < 0.05 *Zfhx3*$^{Sci/+}$ vs *Zfhx3*$^{+/+}$ female, ♂ P < 0.05 *Zfhx3*$^{Sci/+}$ vs *Zfhx3*$^{+/+}$ male, *** P < 0.001, ** P < 0.01, † P < 0.05 between sexes, ††† P < 0.001 between sexes, # P < 0.05 genotype – sex interaction.

Figure 4: Early weight gain of female *Zfhx3*$^{Sci/+}$ mice is lower than wildtype littermates, and driven by lower lean mass.
The *Sci* mutation in female mice inhibits overall weight gain (A), driven by lower lean mass (B), but no differences in fat mass (C) or % fat mass (D). Fasted blood glucose was not altered in these *Zfhx3*$^{Sci/+}$ mice at 8 weeks old (E), and neither was urinary corticosterone at 10 weeks, and time of day differences were maintained (F). At 12 weeks old, these mice underwent indirect calorimetry and the second 24 h of measurements were compared to reveal a trend for lower 24 h RER and significantly reduced dark phase RER (G, I), while energy expenditure was reduced in *Zfhx3*$^{Sci/+}$ mice (time course, H; lean mass ANCOVA adjusted, J). Plotted are mean ± SEM with individual values (E, F, I, J). Statistical comparisons are by mixed effects model (REML) with Šídák's multiple comparisons (A-D), Mann-Whitney tests between genotypes (E, F), Wilcoxon matched – pairs tests (between timepoints, F), RM-2-way ANOVA (G, H), unpaired t-tests (I) and ANCOVA adjusting for lean mass (J). A-E, n = 21 – 23. **** P < 0.0001, *** P < 0.001, ** P < 0.01, * P < 0.05, NSD: no significant differences.

Figure 5: Hypothalamic expression of growth axis component genes are altered by the *Sci* mutation.
Expression of growth hormone releasing hormone (*Ghrh*) is lower in *Zfhx3*$^{Sci/+}$ mice arcuate nucleus (ARC, A) but not posterior paraventricular nucleus (PoPVN, D). Expression of somatostatin (*Sst*) is increased in *Zfhx3*$^{Sci/+}$ mice in the ARC (B) but not periventricular nucleus (PeVN, E). Growth hormone receptor (*Ghr*) expression was lower in *Zfhx3*$^{Sci/+}$ mice and at zeitgeber time (ZT) 3 in the ARC (C) but expression did not differ between groups in the paraventricular nucleus (PVN, F). Plotted are mean ± SEM with individual values overlaid. Example images are shown beneath each plot. Comparisons are by 2-way ANOVA with Šídák's multiple comparisons tests indicated where appropriate. * $P < 0.05$, ** $P < 0.01$, NSD: no significant differences. N = 10 – 12.

Figure 6: Additional hypothalamic gene expression is altered by the *Sci* mutation.
Expression of *Bmal1* in the suprachiasmatic nucleus (SCN) was increased at ZT 15 overall, with an interaction between ZT and genotype, and reduced expression in *Zfhx3*$^{Sci/+}$ mice at ZT 15 only (A). Expression of *Pomc* in the arcuate nucleus (ARC) approached a significant reduction in *Zfhx3*$^{Sci/+}$ mice (B), and ARC expression of *Npy* was overall reduced in *Zfhx3*$^{Sci/+}$ mice (C). Expression of *Gpr50* was increased overall in the ventricular ependymal layer, with pairwise comparisons reaching significance at ZT 15. Plotted are mean ± SEM with individual values overlaid. Example images are shown beneath each plot. Comparisons are by 2-way ANOVA with Šídák's multiple comparison tests indicated where appropriate. *Npy* data were log transformed for statistical comparison. * $P < 0.05$, ** $P < 0.01$, *** $P < 0.001$. NSD: no significant differences. N = 10 – 12.

Table 1: Brain regions investigated for mRNA expression.
In situ hybridisation was carried out on coronal brain sections spanning the hypothalamus. Investigation for mRNA expression was carried out in different hypothalamic brain regions and quantified in figures 5 – 7. +: expression detected and quantified, -: expression not detected. SCN: suprachiasmatic nucleus, ARC: arcuate nucleus, PVN: paraventricular nucleus, PoPVN: posterior paraventricular nucleus, PeVN: periventricular nucleus, DMH: dorsomedial hypothalamus.